Matter and Radiation at Extremes | RESEARCH ARTICLE | scitation.org/journal/mre

High-repetition-rate few-attosecond high-quality electron beams generated from crystals driven by intense X-ray laser

Cite as: Matter Radiat. Extremes 5, 054401 (2020); doi: 10.1063/5.0004524
Submitted: 11 February 2020 • Accepted: 6 July 2020 •
Published Online: 30 July 2020

Zhenfeng Liang,[1] Baifei Shen,[1,a)] Xiaomei Zhang,[2] and Lingang Zhang[2]

AFFILIATIONS

[1]Department of Physics, Shanghai Normal University, Shanghai 200234, China
[2]State Key Laboratory of High Field Laser Physics, Shanghai Institute of Optics and Fine Mechanics, Chinese Academy of Sciences, Shanghai 201800, China

[a)]**Author to whom correspondence should be addressed:** bfshen@shnu.edu.cn

ABSTRACT

Advances in X-ray laser sources have paved the way to relativistic attosecond X-ray laser pulses and opened up the possibility of exploring high-energy-density physics with this technology. With particle-in-cell simulations, we investigate the interaction of realistic metal crystals with relativistic X-ray laser pulses of parameters that will be available in the near future. A wakefield of the order of TV/cm is excited in the crystal and accelerates trapped electrons stably even though the wakefield is locally modulated by the crystal lattice. Electron injection either occurs at the sharp crystal–vacuum boundary or is controlled by coating the crystal with a high-density film. High-repetition-rate attosecond (20 as) monoenergetic electron beams of energy 125 MeV, charge 100 fC, and emittance 1.6×10^{-9} m rad can be produced by shining MHz X-ray laser pulses of energy 2.1 mJ onto coated crystals several micrometers thick. Such a miniature crystal accelerator, which has high reproducibility and allows sufficient control of the parameters of the electron beams, greatly expands the applications of X-ray free electron lasers. For example, it could serve as an ideal electron source for ultrafast electron diffraction and ultrafast electron microscopy to achieve attosecond resolution.

Thanks to the development of high-intensity short-pulse optical lasers, we have gained valuable insights into high-energy-density physics.[1] One of the promising applications of this technology is laser wakefield acceleration (LWFA), where a stable wakefield of the order of GV/cm is excited in a gas plasma by an intense optical laser.[2–4] Electrons can be ejected into the wake due to nonlinear bubble evolution[5] or via controlled-injection techniques such as the colliding-pulse mechanism,[6–9] ionization injection,[10–12] or the density-transition technique.[13–17] These trapped electrons can be accelerated up to several GeV[12,18] and have micrometer milliradian emittance[7] and femtosecond duration.[19] Importantly, electron beams with durations of hundreds of attoseconds could be generated through either a strong chirp of the betatron frequency[20] or elaborate plasma-density modulation.[21,22] Such ultrashort electron beams are useful for ultrafast electron diffraction and ultrafast electron microscopy.[23–25]

Currently, another novel light source, coherent X-ray pulse generation, is developing rapidly. On the one hand, present X-ray free electron lasers (XFELs) can generate coherent photon pulses with 10^{12}–10^{13} photons per pulse,[26] wavelengths from 100 nm to less than 0.1 nm,[27] and controllable polarization from linear[28] to circular.[29] Furthermore, XFELs with a full width at half maximum (FWHM) of 200 attoseconds have been successfully generated,[30] and durations of several tens of attoseconds could be achieved via a chirped-laser-enhanced high-gain XFEL.[31] On the other hand, a scheme for generating ultrashort, intense, coherent X-ray pulses with an optical laser has been proposed whereby a single-cycle optical laser pulse is generated by thin-film compression[32] and this is then upconverted into an attosecond intense X-ray laser pulse by an over-critical solid target.[33] In combination with hard-X-ray focusing technology that can focus X-ray beams to 7 nm at 20 keV,[34] relativistic attosecond X-ray laser pulses can be obtained. Thus, it is practically possible to use relativistic attosecond X-ray laser pulses to explore high-energy-density physics, such as X-ray LWFA.[35–39]

Since X-ray LWFA usually occurs in solid-density plasma, a strong wakefield of the order of TV/cm can be excited, whether in

crystals,[35] nanotubes,[36] or uniform plasma.[36–40] In uniform plasma, when the laser and plasma wavelengths have the same ratio, the electron energy gains via X-ray LWFA are similar to those via optical LWFA over one dephasing length, while the electron emittance in X-ray LWFA is of the order of 10^{-2} mm mrad, almost three orders of magnitude smaller than that of optical LWFA, because the electron emittance is proportional to the wavelength.[36] Moreover, in plasmas with free electrons and a lattice of ions, one-dimensional particle-in-cell (PIC) simulations have proved that the central wakefield dynamics are not affected by the ionic lattice force, where the wavelength of the X-ray laser is 100 times the ion spacing.[38]

In this letter, we investigate the production of attosecond high-quality electron beams by the interaction of a realistic metal crystal with relativistic X-ray laser pulses having parameters that will be available in the near future. As stable materials, crystals are filled with a large number of electrons. However, most of these electrons are bound around ions, forming a periodic crystal lattice. Taking this lattice into account, we find that although a wakefield excited in a crystal is modulated locally by the crystal lattice, the injected electrons can be accelerated stably. High-repetition-rate high-quality attosecond electron beams can be generated by shining a MHz XFEL onto a micrometer-thick crystal with or without a coating. This miniature crystal accelerator, a simple converter from X-ray laser to energetic electron beam, greatly expands the applications of XFEL. For example, it could serve as an ideal electron source for ultrafast electron diffraction and ultrafast electron microscopy to achieve attosecond resolution.

The 2D PIC code EPOCH[41] was employed to investigate the generation of attosecond electron pulses in crystals driven by an X-ray laser, as shown in Fig. 1(a). When a relativistic X-ray laser pulse passes through a crystal, what the X-ray actually "sees" is a set of periodically distributed ions and electrons. The electrons, which are initially bound in the lattice, immediately behave like free electrons due to Coulomb-barrier suppression ionization[42] induced by the intense X-ray electric field. Here, to study the interaction of the crystal with the intense X-ray laser, we take a Cu crystal with a lattice spacing of $d = 0.36$ nm, bound electron clouds of diameter 0.1 nm, and an average electron density of $n_0 = 2.45 \times 10^{30}$ m^{-3} as an example. To model this Cu crystal, we set the following conditions in the simulations: (1) ions and electrons are periodically distributed along the x- and y-directions, with a period equal to the lattice spacing; (2) one positive macroparticle is located at the center of each cell to represent one lattice ion and 27 macroparticles with negative charge, representing lattice electrons, are distributed nearby; (3) the positions of electrons are set to ensure that the average electron density is $n_0 = 2.45 \times 10^{30}$ m^{-3}. Since the role of the crystal lattice is significant when the X-ray wavelength is comparable to the lattice spacing, an X-ray wavelength $\lambda_0 = d = 0.36$ nm (a photon energy of 3.44 keV) is chosen. The X-ray laser is linearly polarized and has a normalized vector potential $a_0 = 3$, corresponding to an intensity $I_0 = 9.5 \times 10^{25}$ W/cm^2. This laser has a Gaussian temporal profile with a FWHM of 20 as and a Gaussian transverse profile with a beam waist radius of 10.8 nm. The total energy of the X-ray laser pulse is 2.1 mJ, corresponding to a photon pulse with photon number 3.8×10^{12}. It is noteworthy that such an X-ray laser will be practically available in the future if XFELs can be well focused and further compressed with the technologies mentioned above.[31,34]

The simulation box is 90×65 nm^2, which corresponds to a moving window with 5000×3600 cells. As Fig. 1(b) shows, the

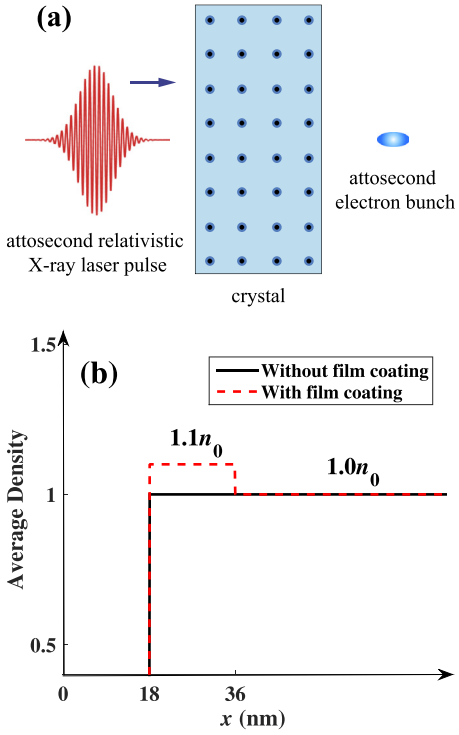

FIG. 1. (a) A sketch of attosecond electron generation in a crystal driven by a relativistic attosecond X-ray laser. The crystal, which has an average density $n_0 = 2.45 \times 10^{30}$ m^{-3}, consists of periodically distributed electrons (blue dots) and ions (black dots) with an equal spacing of 0.36 nm along the x- and y-directions. (b) Average electron density profiles in crystals without (black solid line) and with (red dashed line) a high-density ($1.1n_0$) film of thickness 18 nm.

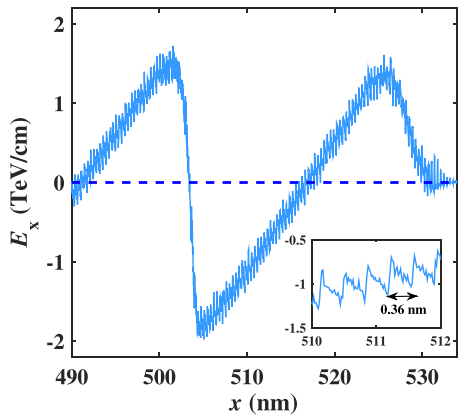

FIG. 2. Lineout of the longitudinal wakefield E_x at $y = 0$ after X-ray propagation of 1.8 fs (the timing of X-ray laser reaching the crystal is 0.12 fs). As the inset shows, E_x exhibits periodic modulation every 0.36 nm due to the local ionic electrostatic fields in the crystal lattice.

crystal location is $x > 36$ nm. An absorptive boundary condition is employed for both particles and fields. In the simulations, quantum radiative effects are not included, since the calculated $I_0\lambda_0^{4/3} = 2.4\times10^{21}$ W/cm^2 μm$^{4/3}$ is two orders of magnitude lower than the critical value 2.65×10^{23} W/cm^2 μm$^{4/3}$ where radiation reaction dominates in plasmas.[43] In theory, when the electron temperature is 10 keV, the electron–ion collision frequency is about 2×10^{14} s^{-1}. The corresponding electron mean free path is about 1.5 μm, which is comparable to the electron acceleration distance studied in the simulation. Therefore, an electron–ion collision will occur on average once during the acceleration. Fortunately, since the electrons have good collimation in the acceleration process, the collision probability becomes smaller for electrons in the middle of the lattice for electrons in the middle of the lattice.

First, we study the characteristics of the wakefield in crystals driven by X-ray laser pulses. When the intense X-ray laser passes through the crystal, these "free electrons" are expelled by the ponderomotive force. Due to the existence of the ionic electrostatic field, some electrons remain bound around the crystal lattice. Nonetheless, spherical bubbles with some residual electrons are formed, and the radius of these bubbles is $R = 12$ nm, as shown in Fig. 2. The lineout of the longitudinal wakefield E_x exhibits a linear slope as a whole and has a maximum at 1.6 TV/cm at the end of the first bubble. However, as the inset of Fig. 2 shows, the longitudinal wakefield E_x periodically oscillates every 0.36 nm, and the closer it is to the ions in the crystal lattice, the more strongly the wakefield is locally modulated. This modulation is due to the strong electrostatic fields around the ions in the crystal lattice. Similarly, the transverse wakefield E_y is also modulated because the crystal lattice is periodically distributed in two dimensions. Although the longitudinal wakefield oscillates due to the crystal lattice, the scalar potential of the wake is not modulated along the x axis, and this is beneficial for stable electron acceleration.

Next, we study electron injection in such a crystal driven by an intense X-ray laser. Although electron trapping due to a steep plasma–vacuum boundary was suggested almost three decades ago,[44] it has so far received little attention because it is difficult for a sharp gaseous plasma–vacuum interface to exist in the case of optical LWFA. However, for X-ray LWFA in crystals, there is naturally a sharp crystal–vacuum boundary due to the stability of the crystal. Thus, we explore the injection mechanism at this sharp crystal–vacuum boundary. As shown in Fig. 3, when the X-ray laser irradiates the crystal, electrons are pushed into the crystal by the ponderomotive

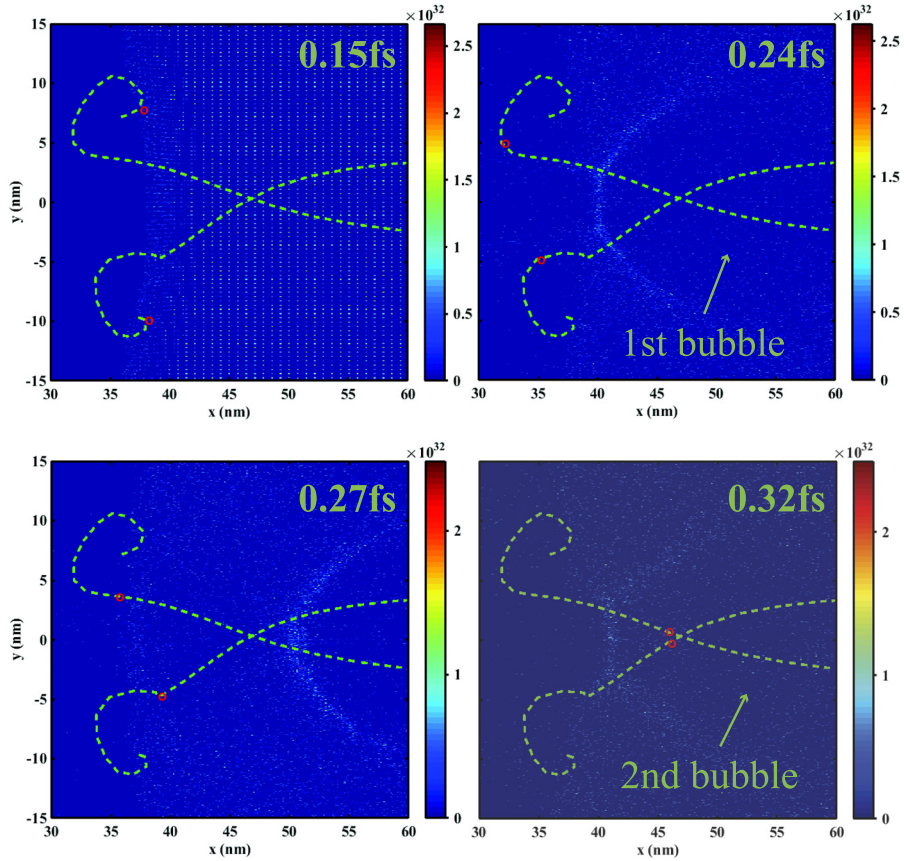

FIG. 3. A series of snapshots from the injection process at the crystal–vacuum boundary in the case of X-ray LWFA in a crystal. The trajectories are for two tracked macroparticles. Each red circle represents one macroparticle's position at the time of the snapshot, and the green line indicates the complete trajectory of the macroparticle. The timing of the X-ray laser reaching the crystal is 0.12 fs and the crystal–vacuum boundary is at $x = 36$ nm.

force, and a strong ionic electrostatic field is generated. Under the effect of this ionic static field, electrons are pulled back towards the vacuum. With the propagation of the X-ray into the crystal, a bubble with some electrons is gradually formed, and numerous electrons accumulate at the end of this bubble. This spike in the electron density produces a large transverse deceleration field, inhibiting further electron accumulation and even leading some electrons to expand towards the vacuum. When these electrons that are moving towards the vacuum come back to the crystal, they form the end of the second bubble. Some electrons that were initially located near the crystal surface, such as the tracked electrons shown by red circles in Fig. 3, enter into the vacuum during the formation of the first bubble, resulting in a phase lag with respect to those electrons that do not enter into the vacuum. Thus, there is not enough time for them to form the end of the first bubble. However, due to the phase lag, these electrons stay in the second bubble as it is gradually formed. With the propagation of the wake, these electrons are eventually trapped in the second bubble and start to gain energy from the wakefield. It is noteworthy that the electron injection is stable due to the stability of the crystal and therefore has high reproducibility.

As Fig. 4 shows, after 2.6 μm of acceleration, the trapped electrons obtain a maximum energy of 78 MeV. The total charge Q of the electron beam is more than 400 fC. The electron distribution in phase space shows that the electron beam length l is 30 nm, corresponding to a pulse duration of 100 as. The transverse size of the electron beam is 10 nm and its normalized emittance is about 2.7×10^{-9} m rad according to the expression for the beam emittance $\varepsilon_{N\_rms} = \langle\gamma\beta\rangle\sqrt{\langle y^2\rangle\langle y'^2\rangle - \langle yy'\rangle^2}$, where $\gamma\beta$ is the momentum, $y' = p_y/p_x$, and p_x and p_y are the longitudinal and transverse momenta, respectively.

Although there is a high reproducibility for the generated attosecond electron beams that are injected into the second bubble at the crystal–vacuum interface, an electron beam source with tunable parameters, such as charge and beam length, is much desired. For X-ray LWFA in crystals, the density-transition technique, which controls electron injection by the density difference before and after the transition,[15–17] may be very suitable for achieving sufficient control over the parameters of the electron beams, although this technique was initially proposed for optical LWFA in gas plasma.[13,14] For crystals, a sharp density transition in which the length of the plasma density changes is much less than the plasma wavelength can be easily achieved by artificially coating the crystal with a film. Moreover, the density difference can be tuned by choosing films of different densities.

Here, a high-density Ag film with periodically distributed ions and electrons, having a thickness of 18 nm and an average density of $1.1n_0$, is considered. When the crystal surface is coated with this film, a sharp downward density transition is formed at the crystal–film interface, as indicated by the red dashed line in Fig. 1(b). In the coated crystal, no electrons are trapped in the first bubble before it meets the density transition. Just after the first bubble goes through the density transition, some electrons are injected into the first bubble. From a kinetic point of view, the injection mechanism can be understood as follows. When the X-ray laser passes through the density transition, some electrons that are initially in the high-density film close to the interface are pushed into the crystal by the X-ray ponderomotive force. These electrons

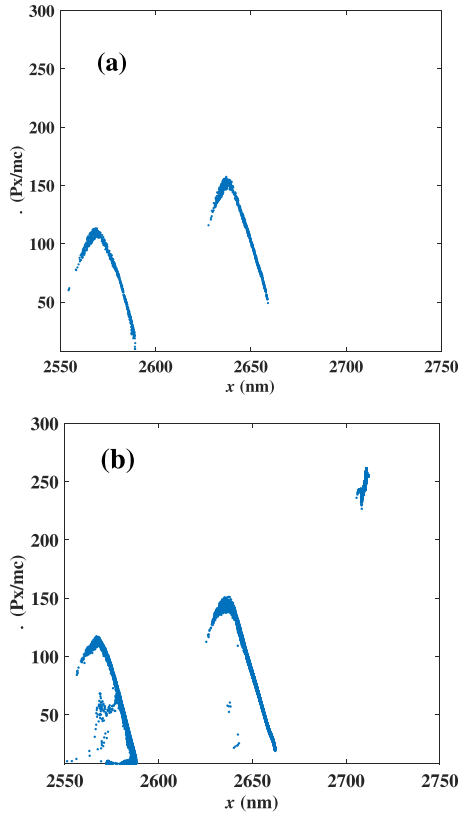

FIG. 4. Electron distribution in phase space (x vs p_x) after 2.6 μm of acceleration. Panels (a) and (b) represent the accelerated electrons in the case of a crystal without and with a coating film of thickness 18 nm, respectively. It is clear that electrons are injected into the second bubble in the case of the uncoated crystal while the electrons are trapped in the first and second bubbles in the case of the coated crystal.

are then pulled back into the higher density film by the ionic electrostatic field. After they return into the film, the forward-moving wakefield accelerates them and changes their direction. Thus, these electrons are injected into the bubble.

The electron distribution in phase space after 2.6 μm of acceleration is shown in Fig. 4. Aside from the electron in the second bubble, there is one bunch of electrons in the first bubble. Here, we only consider the electrons in the first bubble, which are injected by the density transition and gain substantial energy. These electrons have a maximum longitudinal momentum p_x of about $260m_ec$, and the total charge Q of the electron beam is about 100 fC. The electron beam has a longitudinal size of 6.0 nm, which means that its pulse width is 20 as. The transverse size of the electron beam is 5 nm and its normalized emittance is 1.6×10^{-9} m rad. It is worth noting that the parameters of the electron beams produced by X-ray LWFA are tunable by using different densities of coating film on the crystal. With higher density films, the electron charge and electron beam length are greater, while the electron charge and electron beam length are smaller with lower density films. This is similar to the effect seen in optical LWFA in gas plasma.[15–17]

We now discuss the angle between the laser propagation direction and the crystal axis. On the one hand, the index of refraction of the medium for X-rays is $n = 1 - R\lambda^2 F_0/(2\pi V)$. Here $R = 2.817\,94 \times 10^{-6}$ nm is the classical radius of the electron, V is the volume of the unit cell, and F_0 is a structure factor. Depending on the wavelength and the structure factor, the order of magnitude of the refractive index varies from 10^{-5}–10^{-7}. Thus, the effect of the crystal structure on the propagation velocity of the X-rays is negligible, and the grazing angle should not be considered to avoid specular reflection of the X-rays. However, it is worth noting that if electrons are accelerated to GeV or even TeV energies, the crystal structure should be considered carefully, because slowing the group velocity will lead electrons to dephase early. On the other hand, according to the dynamical theory of X-ray diffraction, the intensity reflectivity is large when the incident angle of the X-rays is around the Bragg angle and within the angular Darwin width. Thus, to decrease the reflectivity, the incident angle should be far from the Bragg angle.

In summary, we studied X-ray laser wakefield acceleration in realistic metal crystals using 2D PIC simulations. By mimicking a crystal with periodically distributed electrons and ions along the x- and y-directions, the effects of the crystal lattice on X-ray laser wakefield acceleration are taken into account. In the crystal, a wakefield of the order of TV/cm is excited and can accelerate injected electrons stably even though the wakefield is locally modulated by the crystal lattice. Electron injection at the sharp crystal–vacuum boundary is stable, and it is very easy to control the electron injection by using different densities of film coating on the crystal to adjust the density difference. With MHz X-ray laser pulses, high-repetition attosecond electron beams with low emittance and low energy spread are generated from a crystal chip with a thickness of several micrometers. Such a miniature crystal accelerator, which has high reproducibility and allows sufficient control of the parameters of the electron beams, greatly expands the applications of XFEL. For example, it could serve as an ideal electron source for ultrafast electron diffraction and ultrafast electron microscopy with attosecond resolution.

ACKNOWLEDGMENT

This work was supported by the Ministry of Science and Technology of the People's Republic of China (Grant Nos. 2018YFA0404803 and 2016YFA0401102) and the National Science Foundation of China (Grant No. 11935008).

REFERENCES

[1]R. P. Drake, *High Energy Density Physics* (Springer, Berlin, 2006).
[2]T. Tajima and J. M. Dawson, "Laser electron accelerator," Phys. Rev. Lett. **43**, 267 (1979).
[3]A. Pukhov and J. Meyer-ter-Vehn, "Laser wake field acceleration: The highly nonlinear broken-wave regime," Appl. Phys. B **74**, 355 (2002).
[4]W. Lu, M. Tzoufras, C. Joshi *et al.*, "Generating multi-GeV electron bunches using single stage laser wakefield acceleration in a 3D nonlinear regime," Phys. Rev. Spec. Top.: Accel. Beams **10**, 061301 (2007).
[5]S. Kalmykov, S. A. Yi, V. Khudik *et al.*, "Electron self-injection and trapping into an evolving plasma bubble," Phys. Rev. Lett. **103**, 135004 (2009).
[6]E. Esarey, R. F. Hubbard, W. P. Leemans *et al.*, "Electron injection into plasma wake fields by colliding laser pulses," Phys. Rev. Lett. **79**, 2682 (1997).
[7]J. Faure, C. Rechatin, A. Norlin *et al.*, "Controlled injection and acceleration of electrons in plasma wakefields by colliding laser pulses," Nature **444**, 737 (2006).
[8]X. Davoine, E. Lefebvre, C. Rechatin *et al.*, "Optical injection producing monoenergetic, multi-Gev electron bunches," Phys. Rev. Lett. **102**, 065001 (2009).
[9]C. Rechatin, J. Faure, A. Ben-Ismail *et al.*, "Controlling the phase-space volume of injected electrons in a laser-plasma accelerator," Phys. Rev. Lett. **102**, 164801 (2009).
[10]A. Pak, K. A. Marsh, S. F. Martins *et al.*, "Injection and trapping of tunnel-ionized electrons into laser-produced wakes," Phys. Rev. Lett. **104**, 025003 (2010).
[11]C. McGuffey, A. G. R. Thomas, W. Schumaker *et al.*, "Ionization induced trapping in a laser wakefield accelerator," Phys. Rev. Lett. **104**, 025004 (2010).
[12]C. E. Clayton, J. E. Ralph, F. Albert *et al.*, "Self-guided laser wakefield acceleration beyond 1 GeV using ionization-induced injection," Phys. Rev. Lett. **105**, 105003 (2010).
[13]S. Bulanov, N. Naumova, F. Pegoraro *et al.*, "Particle injection into the wave acceleration phase due to nonlinear wake wave breaking," Phys. Rev. E **58**, R5257 (1998).
[14]H. Suk, N. Barov, J. B. Rosenzweig *et al.*, "Plasma electron trapping and acceleration in a plasma wake field using a density transition," Phys. Rev. Lett. **86**, 1011 (2001).
[15]H. Ekerfelt, M. Hansson, I. Gallardo González *et al.*, "A tunable electron beam source using trapping of electrons in a density down-ramp in laser wakefield acceleration," Sci. Rep. **7**, 12229 (2017).
[16]A. M. de la Ossa, Z. Hu, M. J. V. Streeter *et al.*, "Optimizing density down-ramp injection for beam-driven plasma wakefield accelerators," Phys. Rev. Accel. Beams **20**, 091301 (2017).
[17]S. A. Samant, A. K. Upadhyay, and S. Krishnagopal, "High brightness electron beams from density transition laser wakefield acceleration for shortwavelength free-electron lasers," Plasma Phys. Control. Fusion **56**, 095003 (2014).
[18]W. P. Leemans, A. J. Gonsalves, H. S. Mao *et al.*, "Multi-GeV electron beams from capillary-discharge-guided subpetawatt laser pulses in the self-trapping regime," Phys. Rev. Lett. **113**, 245002 (2014).
[19]O. Lundh, J. Lim, C. Rechatin *et al.*, "Few femtosecond, few kiloampere electron bunch produced by a laser–plasma accelerator," Nat. Phys. **7**, 219 (2011).
[20]M. J. H. Luttikhof, A. G. Khachatryan, F. A. van Goor *et al.*, "Generating ultrarelativistic attosecond electron bunches with laser wakefield accelerators," Phys. Rev. Lett. **105**, 124801 (2010).
[21]F. Y. Li, Z. M. Sheng, Y. Liu *et al.*, "Dense attosecond electron sheets from laser wakefields using an up-ramp density transition," Phys. Rev. Lett. **110**, 135002 (2013).
[22]M. P. Tooley, B. Ersfeld, S. R. Yoffe *et al.*, "Towards attosecond high-energy electron bunches: Controlling self-injection in laser-wakefield accelerators through plasma-density modulation," Phys. Rev. Lett. **119**, 044801 (2017).
[23]M. Gao, C. Lu, H. Jean-Ruel *et al.*, "Mapping molecular motions leading to charge delocalization with ultrabright electrons," Nature **496**, 343 (2013).
[24]J. Yang, J. Beck, C. J. Uiterwaal *et al.*, "Imaging of alignment and structural changes of carbon disulfide molecules using ultrafast electron diffraction," Nat. Commun. **6**, 8172 (2015).
[25]G. Sciaini, M. Harb, S. G. Kruglik *et al.*, "Electronic acceleration of atomic motions and disordering in bismuth," Nature **458**, 56 (2009).
[26]G. Geloni, E. Saldin, L. Samoylova *et al.*, "Coherence properties of the European XFEL," New J. Phys. **12**, 035021 (2010).
[27]C. Pellegrini, A. Marinelli, and S. Reiche, "The physics of x-ray free-electron lasers," Rev. Mod. Phys. **88**, 015006 (2016).
[28]P. Emma, R. Akre, J. Arthur *et al.*, "First lasing and operation of an ångstrom-wavelength free-electron laser," Nat. Photonics **4**, 641 (2010).
[29]A. A. Lutman, J. P. MacArthur, M. Ilchen *et al.*, "Polarization control in an X-ray free-electron laser," Nat. Photonics **10**, 468 (2016).
[30]S. Huang, Y. Ding, Y. Feng *et al.*, "Generating single-spike hard x-ray pulses with nonlinear bunch compression in free-electron lasers," Phys. Rev. Lett. **119**, 154801 (2017).
[31]Z. Wang, C. Feng, and Z. Zhao, "Generating isolated terawatt-attosecond x-ray pulses via a chirped-laser-enhanced high-gain free-electron laser," Phys. Rev. Accel. Beams **20**, 040701 (2017).

[32]G. Mourou, "Single cycle thin film compressor opening the door to Zeptosecond-Exawatt physics," Eur. Phys. J. Spec. Top. **223**, 1181 (2014).
[33]N. Naumova, I. Sokolov, J. Nees *et al.*, "Attosecond electron bunches," Phys. Rev. Lett. **93**, 195003 (2004).
[34]H. Mimura, S. Handa, T. Kimura *et al.*, "Breaking the 10 nm barrier in hard-X-ray focusing," Nat. Phys. **6**, 122 (2009).
[35]T. Tajima and M. Cavenago, "Crystal X-ray accelerator," Phys. Rev. Lett. **59**, 1440 (1987).
[36]X. Zhang, T. Tajima, D. Farinella *et al.*, "Particle-in-cell simulation of x-ray wakefield acceleration and betatron radiation in nanotubes," Phys. Rev. Accel. Beams **19**, 101004 (2016).
[37]T. Tajima, "Laser acceleration in novel media," Eur. Phys. J. Spec. Top. **223**, 1037 (2014).
[38]S. Hakimi, T. Nguyen, D. Farinella *et al.*, "Wakefield in solid state plasma with the ionic lattice force," Phys. Plasmas **25**, 023112 (2018).
[39]B. Svedung Wettervik, A. Gonoskov, and M. Marklund, "Prospects and limitations of wakefield acceleration in solids," Phys. Plasmas **25**, 013107 (2018).
[40]T. Tajima, K. Nakajima, and G. Mourou, "Laser acceleration," Riv. Nuovo Cim. **40**, 1 (2017).
[41]T. D. Arber, K. Bennett, C. S. Brady *et al.*, "Contemporary particle-in-cell approach to laser-plasma modelling," Plasma Phys. Control. Fusion **57**, 113001 (2015).
[42]S. Augst, D. D. Meyerhofer, D. Strickland *et al.*, "Laser ionization of noble gases by Coulomb-barrier suppression," J. Opt. Soc. Am. B **8**, 858 (1991).
[43]S. V. Bulanov, T. Z. Esirkepov, J. Koga *et al.*, "Interaction of electromagnetic waves with plasma in the radiation-dominated regime," Plasma Phys. Rep. **30**, 196 (2004).
[44]S. V. Bulanov, I. N. Inovenkov, N. M. Naumova *et al.*, "Excitation of a relativistic Langmuir wave and electron acceleration through the action of an electromagnetic pulse on a collisionless plasma," Sov. J. Plasma Phys. **16**, 444 (1990).